

# Combined Order Parameters Response in a Charge-Density Wave Superconductor

Aleksej V. Mialitsin<sup>1,2,3\*</sup>, Ilia A. Solov'yov<sup>4,5</sup>, Anna I. Tóth<sup>6</sup>, Igor I. Mazin<sup>7</sup>,  
Andriy H. Nevidomskyy<sup>2,8</sup>, Brian S. Dennis<sup>2,3</sup>, Girsh Blumberg<sup>2,3</sup>

August 14, 2012

<sup>1</sup>National Renewable Energy Laboratory, Golden, CO 80401, USA

<sup>2</sup>Department of Physics and Astronomy, Rutgers University, Piscataway, NJ 08854, USA

<sup>3</sup>Bell-Laboratories, Alcatel-Lucent, Murray Hill, NJ 07974, USA

<sup>4</sup>Beckman Institute for Advanced Science and Technology, University of Illinois Urbana Champaign, Urbana, IL 61801, USA

<sup>5</sup>A. F. Ioffe Physical-Technical Institute, Russian Academy of Sciences, St. Petersburg 194021, Russian Federation

<sup>6</sup>Institute of Solid State Physics, Vienna University of Technology, 1040 Vienna, Austria

<sup>7</sup>Naval Research Laboratory, Washington, DC 20375, USA

<sup>8</sup>Department of Physics and Astronomy, Rice University, Houston, TX 77005, USA

---

\*Corresponding author (e-mail): aleksej.mialitsin@nrel.gov

## Abstract

Coexistence of different types of electronic orderings in a solid has always been a subject of intense interest among physicists. Electronic orderings can be either competitive, even mutually exclusive, as is the case of superconductivity and magnetism, or cooperative, mutually reinforcing, as in the case of magnetic and electric moments in ferroelectric materials. In niobium-di-selenide ( $\text{NbSe}_2$ ), conventional superconductivity is known to occur inside the charge-density wave phase. Such a system provides a great example for studying coexistence and interplay of electronic orderings. By employing Raman scattering we shed light on the low-temperature electronic state in  $\text{NbSe}_2$ , which is characterized by emergent electronic excitations. We show that, contrary to the common belief, the collective excitation in the combined phase reflects an intriguing symbiosis between the two order parameters, which manifests itself in a combined order parameters response in the inelastically scattered spectra.

Niobium-di-selenide is a metallic compound of hexagonal symmetry and a type-II superconductor, whose real and reciprocal space structure is illustrated in Fig. 1 *a-b*. Its quasi-two-dimensional electron bands reflect its layered composition. Its critical transition temperature  $T_c$  is 7.2 K (1). NbSe<sub>2</sub> has attracted significant attention in the context of magnetic flux vortices studies in its mixed state regime (2). Notably, NbSe<sub>2</sub> also belongs to the family of transition metal chalcogenides that host a two dimensional charge-density wave (CDW) below a certain ordering temperature  $T_{\text{CDW}}$ , which in NbSe<sub>2</sub> is about 33 K (3). CDW ground state is realized when the electronic charge in a solid prefers to deviate from the homogenous state and forms an oscillating pattern in order to reduce the electronic kinetic energy. The resulting wave of electron density usually couples electrostatically to the ionic lattice (electron-phonon coupling) causing the latter to distort, which leads to an increase in elastic energy. The CDW can thus be thought of as a cooperative effect of the electrons and the lattice, whose periodic distortion is such that it minimizes the free energy of the entire system.

Well established in the quasi-one-dimensional case, the CDW transition is known as the Peierls instability and is observed in the blue bronze K<sub>0.3</sub>MoO<sub>3</sub> (4) and in organic compounds (5). However, an extension of this CDW formation mechanism to higher dimensions is not straight forward; the Fermi surface nesting is rarely obvious and electron-electron coupling (6) may play a much more prominent role. Additionally, the CDW-induced energy gap in the electronic band structure, which renders the quasi-1D materials insulating, has a much subtler appearance in 2D.

Below  $T_c$ , NbSe<sub>2</sub> hosts both the CDW and the superconducting phases, which raises a question of how the two orderings interplay. In the traditional view, both the formation of the CDW state and the Cooper pairs condensation deplete the density of states at the Fermi level  $N(0)$  and hence, CDW competes with superconductivity. This view is corroborated by the report that under applied pressure, when  $T_{\text{CDW}}$  is

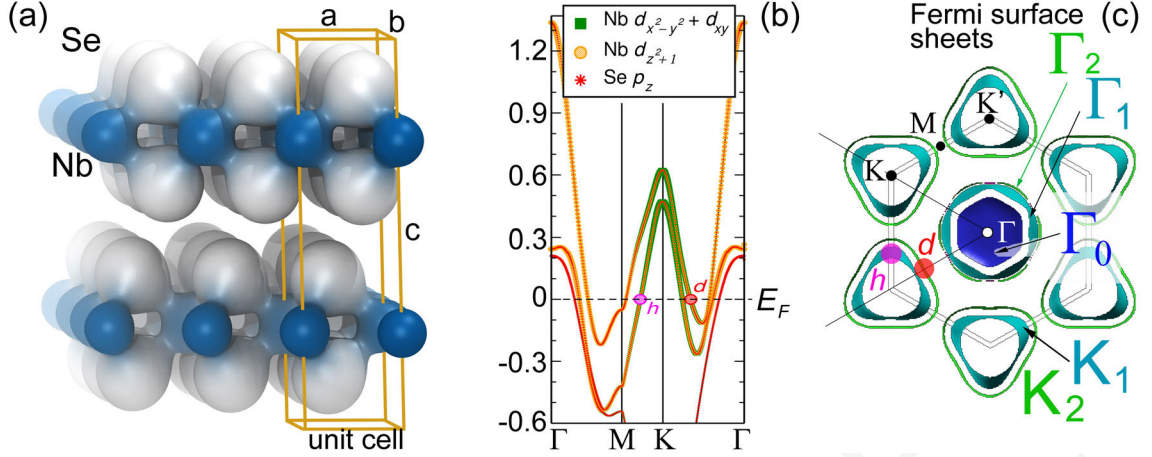


Figure 1: **Crystalline structure and reciprocal space structure of NbSe<sub>2</sub>.** The NbSe<sub>2</sub> lattice with a six-fold symmetry unit cell shown in (a) defines the electronic band structure (b), which has been calculated using the density-functional theory approach (see Methods). Symbol sizes in (b) represent the relative weight of the band characters given by the legend, which specifies to what kind of real combination of the  $p/d$  spherical harmonics around the appropriate ions the projections of the band eigenfunctions have been carried out. The cross-section of the electronic bands with the Fermi level  $E_f$ , the highest occupied energy level in a metal at zero temperature, defines the Fermi surface shown in (c). In NbSe<sub>2</sub>, the Fermi surface consists of multiple sheets: the electronic bands with Nb character form double-walled barrels centered around the  $\Gamma$  and the K-points of the Brillouin zone. Therefore, one has to distinguish between the Fermi surface sheets referred to as the “inner” and the “outer” barrels, denoted in (c) as  $\Gamma_1$ ,  $K_1$ , and  $\Gamma_2$ ,  $K_2$ , respectively. The  $\Gamma_{1,2}$  and the  $K_{1,2}$ -barrels show only a weak  $k$ -dispersion and are thought of as mainly two-dimensional, even though the inner barrels are more warped than the outer barrels. The electronic bands with Se character form the three-dimensional  $\Gamma_0$  Fermi surface sheets enclosing the  $\Gamma$  point, referred to as  $\Gamma$ -“pancakes”. Certain  $k$ -space regions warrant special attention, such as the crossing of the inner K-barrel ( $K_1$ ) with the K-M high symmetry line, denoted as ‘h’, and the crossing of the outer K-barrel ( $K_2$ ) with the  $\Gamma$ -K high symmetry line, denoted as ‘d’.

suppressed, presumably leading to a larger  $N(0)$ , there is a correlated increase in  $T_c$  (7). This situation bears similarity to the cuprates, where charge- and spin-stripes are deemed as detrimental to superconductivity (8).

Electronic Raman scattering measures the spectrum of collective electronic excitations throughout the entire Brillouin zone projected into distinct symmetry channels according to the integral weight of the so called Raman vertices. In a pure one-band

$s$ -wave superconducting state with the energy gap  $\Delta_{SC}$  around the Fermi level, the Raman excitation would result in a distinctly shaped peak at  $2\Delta_{SC}$ , corresponding to the amplitude mode of the superconductor (9). The same effect is expected for the Raman excitations across a CDW energy gap  $\Delta_{CDW}$  (10). The case of the interplay between superconductivity and CDW offers the possibility to selectively turn superconductivity on and off by applying magnetic field while keeping the temperature constant (this is in difference to pressure that, in principle, affects both CDW and superconductivity through the deformation of electronic bands).

Consider a NbSe<sub>2</sub> crystal at a sub- $T_c$  temperature subject to a magnetic field stronger than the upper critical field value  $H_{c2}$ . In this case, the simple picture of the superconducting and the CDW order parameters being in direct competition leads to a conclusion that the collective CDW mode should be pushed down to a lower frequency, as superconductivity is mixed in by reducing the magnetic field. Thus, one expects a decrease of  $\Delta_{CDW}$  inhibited by superconductivity as the two order parameters are forced to share the density of states, similar to the case when superconductivity arrests the martensitic transformation in the A15 compounds (11). In the limiting case, when superconductivity is not able to draw on any states already committed to the CDW, a zero effect is expected, i. e., no change in the CDW excitation frequency.

In reality, as observed by Raman scattering the frequency of the collective excitation of the *combined CDW and superconductivity* (CDW+SC) state is higher than  $2\Delta_{CDW}$ . We are able to explain this effect *quantitatively* by a combined action of the two orderings: the superconductivity and CDW instabilities, in the particle-particle and particle-hole channels, respectively, team up to produce a new collective excitation at a higher frequency. This symbiosis occurs on the microscopic level independent of the respective phases origin and whether they compete or cooperate, simply whenever the involved electrons share the same phase space. We note, that this picture

is different from the idea of a dynamical coupling between the two order parameters (12), which would result in a renormalized amplitude mode at an energy smaller than  $2\Delta_{SC}$ .

In this work, we present temperature and magnetic field dependencies of low frequency Raman response from NbSe<sub>2</sub> in its superconducting and CDW ground states. We find the behavior of Raman peaks induced by the respective phase transitions to be consistent with their electronic scattering origin. We assign one of the features, peak C in zero magnetic field, to arise from a combined energy gap  $\Xi$ , formed by the CDW+SC state that is hosted below  $T_c$  on distinct K-point centered Fermi surfaces. The combination of an anisotropic CDW energy gap with an isotropic superconducting energy gap on those Fermi surface sheets helps to reconcile the seemingly conflicting results reported by recent angle resolved photo emission experiments (ARPES) (13, 14). The view of a combined order parameters response is corroborated by a calculation of Raman vertices in the effective mass approximation.

## Results

**NbSe<sub>2</sub> Raman response in the different phases.** In Fig. 2a, evolution of the ‘polarized’ Raman response from the *ab*-plane of the NbSe<sub>2</sub> crystal is shown as a function of temperature. ‘Polarized’ Raman response combines the A<sub>1g</sub> and E<sub>2g</sub> symmetry channels (see Methods). In the normal state, color coded Raman intensity  $\chi''$  peaks sharply at 250, 235, and 30 cm<sup>-1</sup>, the energies corresponding to the single phonon excitations of Raman active optical lattice vibrations. Another broad peak can be found in the 100 to 200 cm<sup>-1</sup> Raman shift range, originating from two-phonon scattering by the anomalously soft acoustic  $\Sigma_1$  phonon branch near its Brillouin zone edge (3, 15, 16). Upon cooling, Raman scattering peaks induced by the low tem-

perature phases appear, first, in the 30-50  $\text{cm}^{-1}$  range below 33 K, due to CDW, and then, in the 10-20  $\text{cm}^{-1}$  range below 8 K, due to superconductivity.

**CDW induced C-peaks.** The CDW excitation was originally observed by Tsang *et al.* (17), and then, polarization resolved by Sooryakumar and Klein (18). Both works interpreted the signature origin as phononic due to an alleged CDW-induced periodic lattice distortion (19). However, X-ray studies failed to reveal any symmetry lowering in NbSe<sub>2</sub> below  $T_{CDW}$  due to crystal structure changes (20). In cases, such as e.g. TaSe<sub>2</sub>, where a periodic lattice distortion has been established (21), the phononic CDW-induced Raman signature consists of four sharp peaks, which correspond to amplitudons and phasons in the respective polarizations. Such phononic signature is significantly different from the CDW-induced signature observed in NbSe<sub>2</sub>, which consists of two broad peaks, one in each polarization geometry, labeled in Fig. 2b as  $C^A$  and  $C^E$ . As experimental evidence for CDWs without periodic lattice distortion continues to accumulate (22) we conjecture that a similar variety occurs in NbSe<sub>2</sub>. The median Raman shift of the C-peaks maxima at about 43  $\text{cm}^{-1}$  corresponds to the  $2\Delta_{CDW}$  value of about 5.3 meV, which is close to the ARPES value of 2.4 meV for single  $\Delta_{CDW}$  (13). The broad tail towards lower frequencies displayed by the C-peaks reflects the CDW energy gap anisotropy mapped in the same reference. When polarization resolved (see Methods), the CDW-induced intensity gains maximal values at the Raman shifts of 41 and 46  $\text{cm}^{-1}$  in the  $A_{1g}$  and  $E_{2g}$  symmetry channels, respectively. This difference arises naturally due to variation of the Raman vertices in the respective symmetry channels, which are described in Discussion.

**Superconductivity-induced G-peaks.** The superconductivity-induced peaks, too, have different energies in the orthogonal polarization geometries. The  $A_{1g}$  Raman

peak  $G^A$  in Fig. 2b, located at the  $20 \text{ cm}^{-1}$  at 3 K, coincides with the doubled energy of the superconducting energy gap  $\Delta_{SC} = 1.1 \text{ meV}$  as established by techniques such as infrared spectroscopy (23) and scanning-tunneling microscopy (24). Normally, the Raman response from the superconducting density fluctuations is expected to be screened in the  $A_{1g}$  symmetry channel (25), but multi-band superconductivity scenarios (26) provide exceptions to the ubiquity of such screening (27), allowing for superconductivity induced Raman response to occur in the  $A_{-1g}$  symmetry channel to occur in certain cases. Notably, multi-band superconductivity also allows for collective sub- $\Delta_{SC}$  excitations (28), which, consequently, would explain the  $G^E$  Raman peak at  $16 \text{ cm}^{-1}$  in the  $E_{2g}$  symmetry channel. Amplitudes and phases oscillations between the superconducting condensates confined to different Fermi surfaces provide parameter space for a variety of resonances similar to the Leggett's mode observed in  $\text{MgB}_2$  (29). More detailed, preferably time-resolved studies of the  $G^E$  mode are necessary for an unambiguous categorization.

## Discussion

**Correlating Raman and ARPES experiments.** Since electronic Raman scattering response represents only a  $k$ -space projection of electronic excitations from various parts of the Brillouin zone, we rely on  $k$ -space resolved information from ARPES experiments (13) regarding the precise  $k$ -space origin of these excitations. *Consistency* of the Raman response with the  $k$ -resolved information about the density of states in the CDW-phase is an important point that can validate or refute our combined order parameters response conjecture. Based on the ARPES map (13), the CDW energy gap is maximum in the hot-spots 'h' and zero in the 'd'-points of the Brillouin zone located on the inner and outer K-barrels Fermi surface sheets,  $K_1$  and

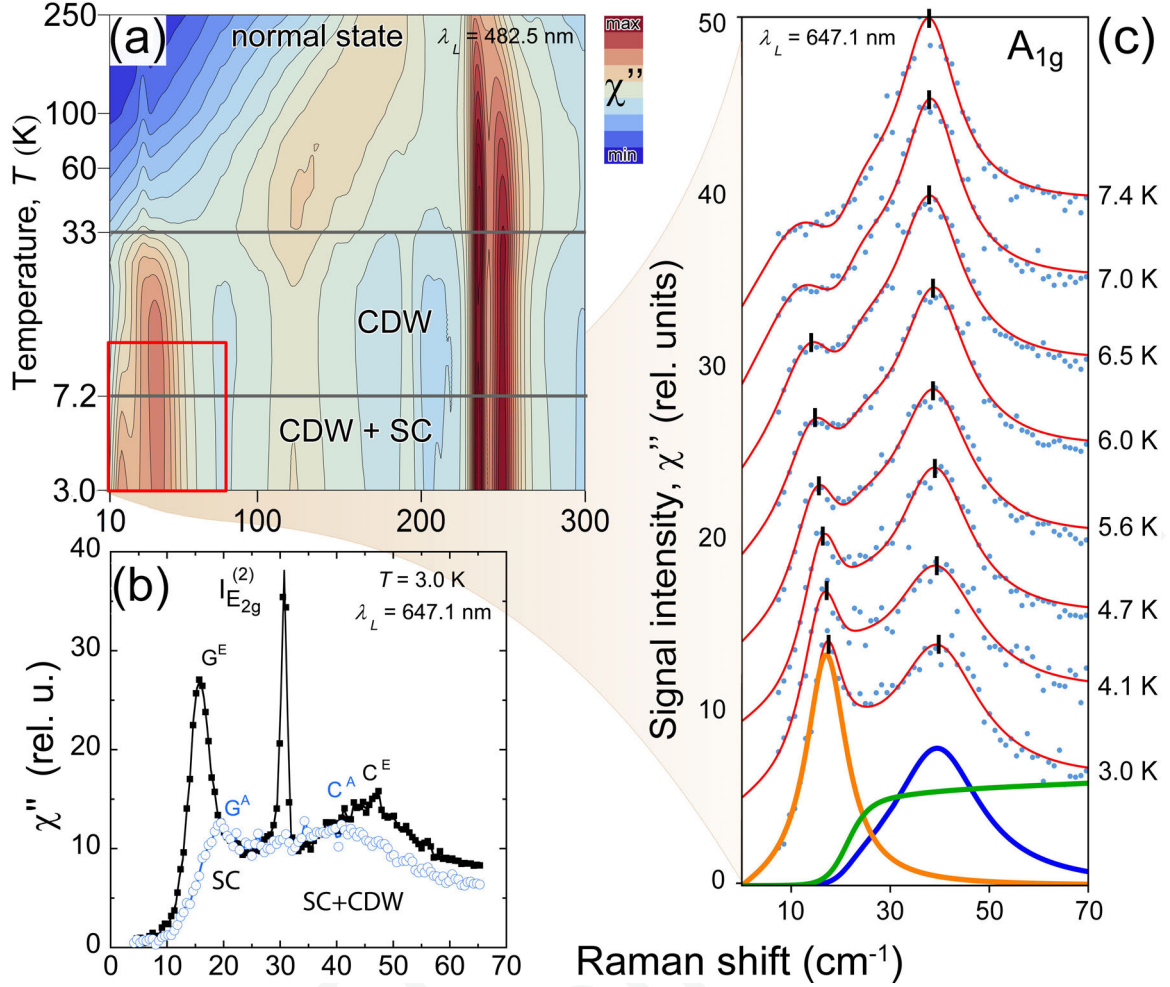


Figure 2: **Raman spectra from NbSe<sub>2</sub>.** (a) Polarized temperature-dependent Raman series generated with the laser excitation wavelength  $\lambda_L = 482$  nm. The three phases: normal state ( $T > 33$  K), the CDW state ( $33 > T > 7.2$  K), and the CDW+SC state ( $T < 7.2$  K) can be distinguished by the phase specific Raman response  $\chi''$  color coded according to the legend. In panel (b), the 3 K spectrum generated off-resonance with  $\lambda_L = 647$  nm is polarization resolved into the  $E_{2g}$  (black squares) and the  $A_{1g}$  (blue circles) contributions, such that the symmetry channel dependent Raman response can be identified. The respective peaks are denoted as  $G^{A,E}$  for superconductivity induced intensity, and as  $C^{A,E}$  for CDW+SC induced intensity. The ionic inter-layer vibration mode is denoted as  $I_{E_{2g}}^{(2)}$ . The parameter space indicated by the red box in (a) is shown in greater detail in panel (c) for the  $A_{1g}$  symmetry channel ( $\lambda_L = 647$  nm). The solid red lines are a fit to the experimental data (blue dots). The fit has been determined by a decomposition according to a phenomenological model (see Supplementary Information). The model consists of the superposition of the  $G^A$  peak (thick orange curve peaking at about  $20$  cm<sup>-1</sup>), the  $C^A$  peak (thick blue curve peaking at about  $40$  cm<sup>-1</sup>), and the superconductivity gapped continuum (thick continuously rising green curve). The maxima of the decomposed peaks are taken as the measure for the G and C peaks positions, indicated with black ticks.

$K_2$ , respectively (see Fig. 1c). Therefore, the  $C^A$  and the  $C^E$  peaks can be due to the CDW excitations only if the Brillouin zone regions around ‘h’ get selected by Raman vertices  $\gamma_n$  in the Raman response projection.

**Invoking Raman vertices to confirm C-peak origin.** In Fig. 3, we show Raman vertices computed in the effective mass approximation (see Supplementary Materials) from the NbSe<sub>2</sub> band structure shown in Fig. 1b. We find that, indeed, the absolute value of both the  $A_{1g}$  and the  $E_{2g}$  Raman vertices peak around the ‘h’-point. The  $A_{1g}$  Raman vertices amplitude becomes maximum in all three equivalent hot-spots on  $K_1$ . The  $E_{2g}$  Raman vertices amplitude is maximized around two out of three hot-spot regions and has a node in the third one. The  $E_{1g}$  Raman vertices amplitude remains low on the  $K_1$  Fermi surface sheet. Correspondingly, no CDW-induced intensity is observed in Raman scattering from the edge of the NbSe<sub>2</sub> crystal (see supplementary Figure S1). All Raman vertices on the  $\Gamma$ -barrels Fermi surface sheets ( $\Gamma_1, \Gamma_2$ ), with the exception of the  $E_{1g}(\Gamma_2)$  vertices, show finite amplitude of the same order of magnitude as the one in the hot-spots regions on the inner K-barrels. From the results of the ARPES measurements, we know that superconductivity exists both on the K- and the  $\Gamma$ -barrels Fermi surface sheets (14). Therefore, the  $\Gamma$ -barrels are the natural locale for the origin of the  $G^A$  peak, which, according to its frequency, is of purely superconductive nature.

**Correlation between the G- and the C-peaks.** In Fig. 2c, we show the temperature dependence of the  $A_{1g}$  Raman response in the parameter space highlighted by the red box in Fig. 2a. A decomposition of the signal intensity according to a phenomenological model (see Supplementary Materials) allows one to fit the data and measure the position of the  $C^A$  and the  $G^A$  peaks, marked with black ticks in Fig. 2c.

These peak positions, together with their  $E_{2g}$  counterparts are shown in Fig. 4 as a function of temperature (panels *c*, *e*) and as a function of magnetic field (panels *b*, *d*). Upon cooling, the  $C^{A,E}$  peaks positions saturate before temperature reaches  $T_c$ , and then increase again, following the emergence of the respective G peaks. As a function of magnetic field, the two peaks, too, are closely correlated. Such correlation implies that we indeed observe a combined Raman scattering response and not necessarily the order parameters themselves. But conclusions about the order parameters underlying the response are still possible, which we proceed to explore.

**Combined order parameters Raman response  $2\Xi$ .** One can understand the evolution of the low-temperature phases induced Raman response if specific peaks are assigned to represent specific energy gaps. For the sake of convenience, consider the  $A_{1g}$  symmetry channel: By comparing spectra taken in high magnetic field to those taken in zero magnetic field (Fig. 4b, 4d), we obtain values for the pure superconductivity and CDW energy gaps independent of each other. The former ( $\Delta_{SC}$ ), is derived from the  $G^A$  peak in the  $H = 0$  T spectra.  $G^A$  originates from the  $\Gamma$ -barrels and, therefore, is unperturbed by the CDW. The latter ( $\Delta_{CDW}$ ), is derived from the  $C^A$  peak position in the  $H > H_{c2}$  spectra, when CDW located on the inner K-barrels remains the only source for electronic excitations, because superconductivity has been suppressed. Thus, the position of the  $C^A$  peak recorded in zero magnetic field reflects a combined response from the electronic excitations corresponding to the superconducting and the CDW order parameters on the inner K-barrels. As such excitations combine in orthogonal channels, the combined energy  $\Xi$  relates to the energy of the constituting excitations,  $\Delta_{CDW}$  and  $\Delta_{SC}$ , as

$$\Xi = \sqrt{\Delta_{SC}^2 + \Delta_{CDW}^2}. \quad (1)$$

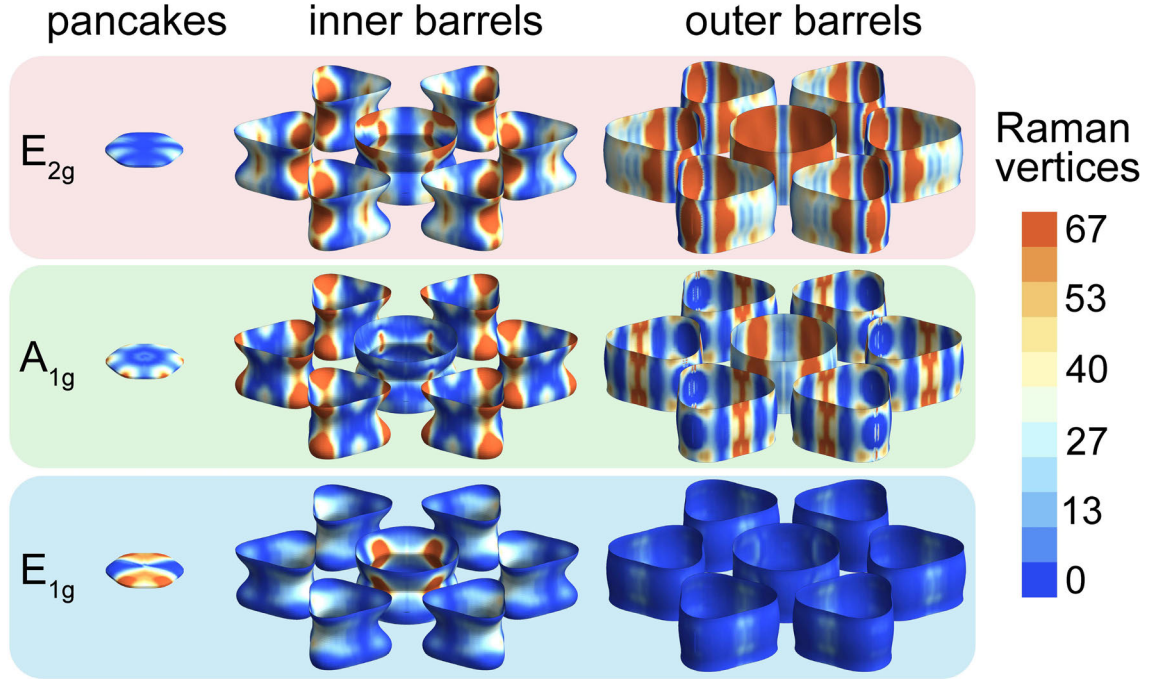


Figure 3: **Raman vertices in NbSe<sub>2</sub>**. The square of the Raman vertices amplitude  $\gamma_n^2$  calculated for the three Raman active symmetry channels  $A_{1g}$ ,  $E_{2g}$ , and  $E_{1g}$  is color coded atop the Fermi surface sheets  $\Gamma_2$  and  $K_2$  (right column, “inner barrels”),  $\Gamma_1$  and  $K_1$  (middle column, “inner barrels”), and  $\Gamma_0$  (left column, “pancakes”).  $A_{1g}$  is the fully symmetric Raman vertices channel corresponding to light scattering from the ‘ab’-plane of the NbSe<sub>2</sub> crystal.  $E_{2g}$  is a non-symmetric channel that results in Raman vertices changing sign under certain space group symmetry operations. Consequently, the squared  $E_{2g}$  Raman vertices amplitudes in the  $E_{2g}$  row have nodes.  $E_{2g}$  symmetry channel, too, refers to scattering from the ‘ab’-plane.  $E_{1g}$  is a non-symmetric Raman vertices channel for scattering from the ‘ac’ or ‘bc’ edges of the NbSe<sub>2</sub> crystal (see Fig. 1b.)

Ref.(14) (meV)	Ref.(13) (meV)	this work (meV)
$\Delta_{LES}(h) = 0.3$	$\Delta_{CDW}(h) = 2.4$	$\sqrt{\Delta_{SC}^2(h) + 2.4^2} - 2.4 = 0.3$ if $\Delta_{SC}(h) = 1.2$
$\Delta_{LES}(d) = 1.2$	$\Delta_{CDW}(d) = 0$	$\underbrace{\sqrt{\Delta_{SC}^2(d) + 0^2} - 0}_{\Xi} = 1.2$ if $\Delta_{SC}(d) = 1.2$

Table 1: Characteristic energies of the low temperature phases in NbSe<sub>2</sub> for selected points in the BZ.

Therefore, by assuming that the superconductivity energy gap on the Nb-orbitals derived K-barrels is the same as that on the  $\Gamma$ -barrels, which too are Nb-derived (Fig. 1b), we predict an expected temperature dependence for  $\Xi$ . It follows from Eq. (1), where  $2\Delta_{SC}$  is given by the Raman shift of the  $G^A$  peak as a function of temperature (Fig. 4a, bottom, solid circles) and  $2\Delta_{CDW}$  is given by the  $C^A(H > H_{c2})$  peak Raman shift. We note that, the  $C^A(H > H_{c2})$  peak frequency is temperature independent below  $T_c$  (Fig. 4a, center, solid square).

**Combined order parameters response vs. Raman shift of the C-peaks.** In Fig. 4a we compare the predicted  $2\Xi$  values (center panel, empty squares) with the experimentally observed position of the  $C^A$  peak that we associate with the combined order parameter (center panel, crosses). Similar comparison is done for the combined order parameter response calculated from the  $G^A$  and  $C^E$  Raman shifts and the  $C^E$  peak position (top panel, empty squares vs. crosses). The comparison shows good agreement of the two quantities in both symmetry channels, thereby proving the three underlying assumptions: i) Low energy Raman scattering from NbSe<sub>2</sub> probes electronic excitations; ii) On the microscopic level, the electrons respond to a “combined order parameter” as described by Eq. (1); and iii) The magnitude of the superconducting energy gap on the K-barrels is close to that on the  $\Gamma$ -barrels. Given that all three assumptions must be fulfilled simultaneously, a fortuitous coincidence of effects of different nature to result in an effect of the exactly same magnitude, appears relatively unlikely.

**Isotropic multiband superconductivity conjecture.** A corollary of the presented model is that the interpretation of NbSe<sub>2</sub> ARPES data by Kiss *et al.* in terms of the superconducting gap anisotropy (14), which would be very unusual for a con-

ventional superconductor, might instead be explained as a combination of an isotropic superconducting energy gap and an anisotropic CDW energy gap. In this picture, the superconducting energy gap is naturally isotropic because NbSe<sub>2</sub> is a phonon mediated *s*-type superconductor. The CDW energy gap is naturally anisotropic because of the nesting geometry of the Fermi surface.

To this end, we note that the conclusion of Ref. (14) in regard to the superconducting energy gap anisotropy is deduced from analyzing spectral renormalization across  $T_c$ . Spectra above and below  $T_c$  are compared by means of the *leading edge shift* (LES) data analysis technique. Usually, the LES energy can be taken to equal to the superconducting gap energy. But the ARPES measurement in question has been performed across the superconducting phase transition *in the presence* of a CDW that, in this particular experiment, has remained undetected.

The findings of Ref. (14) can be summarized as follows: The LES as a function of temperature across the superconductivity phase transition is mainly uniform on the  $\Gamma$ -barrels, with  $\Delta_{LES}(\Gamma_1, \Gamma_2) = 0.9 - 1.1$  meV, anisotropic on the K-barrels with a minimum value of 0.3 meV on the inner K<sub>1</sub>-triangle, where it crosses the K-M direction ('h'-point in Fig. 1 *c*, compare Fig. 4 *a* in (14)), and a maximum value of 1.2 meV on the outer K<sub>2</sub>-triangle along the  $\Gamma$ -K direction ('d'-point).

Borisenko *et al.* (13) were able to specifically measure the CDW gap in NbSe<sub>2</sub>, which was done by comparing ARPES spectra from point *d* on the outer K<sub>2</sub>-barrels to spectra taken from other points in the Brillouin zone. Based on their overall temperature dependence, spectra from the 'd'-point were found to have no CDW gap. By taking point 'd' as a calibration for  $\Delta_{CDW} = 0$ , Borisenko *et al.* find that a CDW gap opens on parts of the inner K<sub>1</sub>-barrel with a maximum in the hot-spot 'h'. Moreover, thanks to a *k*-space resolution of less than  $0.02 \text{ \AA}^{-1}$  the three equivalent 'h' points of each K<sub>1</sub>-triangle are found to be nested by the charge-density wave vectors

$\vec{Q}_{CDW}$  (Fig. 1 in (13)). This correlation between the hot-spots and nesting establishes the anisotropy of the CDW gap: the CDW gap is maximum in nested regions and decreases away from them.

We reconcile the competing findings of the two ARPES studies (Ref. (14) suggests mutual enhancement and Ref. (13) suggests competition between the order parameters) within our concept of the isotropic superconducting gap by summarizing the characteristic energies of the low temperature phases in Table 1. The LES energies across  $T_c$  found by (14) for points ‘d’ and ‘h’ are listed in the first column. The CDW gap energies found by (13) in the same points are listed in the second column. Following the conjecture of combined order parameters response, expected LES energy across the superconducting phase transition is calculated in the third column as it would result from the difference between the energy gap of the CDW+SC order parameter  $\Xi$  and the plain CDW energy gap  $\Delta_{CDW}$ , because it is in fact a CDW to CDW+SC phase transition that occurs across  $T_c$ , and not a normal state to superconducting state phase transition. In the absence of the CDW gap a pure superconductivity order parameter is observed. This condition is fulfilled in point ‘d’. In the hot-spot ‘h’, the experimentally observed LES energy of 0.3 meV is retrieved if the superconducting energy gap in that point,  $\Delta_{SC}(h)$  were to have the magnitude of 1.2 meV. With  $\Delta_{SC}(h) = 1.2$  meV, a magnitude of the combined order parameter energy gap  $\Xi$  of 2.6 meV or  $2\Xi = 43.2$  cm<sup>-1</sup> follows, which is close to the median of the  $C^A$  and  $C^E$  CDW peaks frequencies in zero magnetic field at 3 K (see Fig. 2b).

These considerations infer, that in the scenario of the combined CDW+SC order parameters response the observations of anisotropic LES energies across  $T_c$  (14) are consistent with observations of an anisotropic CDW gap (13) if we assume an isotropic superconducting energy gap on the K-barrels. Incidentally, the energy gap on the K-barrels,  $\Delta_{SC}(K) \approx 1.2$  meV based on this analysis, is of almost the same magnitude,

as the one on the  $\Gamma$ -barrels,  $\Delta_{SC}(\Gamma) \approx 1.1$  meV. This independently confirms our previous assumption about the superconducting gap size on the K-barrels in regard to Raman scattering.

**Fundamental gap on the  $\Gamma_0$  “pancakes” Fermi surface sheets.** Finally, in the combined SC+CDW state the Raman scattering signature from the  $ab$ -plane shows a fundamental gap  $2\Delta_0$  of approximately  $8 \text{ cm}^{-1}$ , as indicated by Raman intensity dropping to absolute zero both in the  $A_{1g}$  and the  $E_{2g}$  symmetry channels (Fig. 2b) below this threshold. This fundamental gap is consistent with gapping of highly resolved STM spectra (30). Since the large gap at the Nb derived FS sheets has been accounted for,  $2\Delta_0$  must reside on the Se derived ‘pancakes’.

**Conclusion.** While our study confirms superconductivity of the conventional type in NbSe<sub>2</sub>, a multi-band superconductivity case emerges, where all five Fermi surface sheets play different roles in regards to electronic excitations observed in various spectroscopies. We find that electronic light scattering within a specific Fermi surface geometry, where the CDW and the superconductive orderings overlap, explains the temperature and magnetic field behavior of Raman spectra if the low frequency Raman signal is viewed as a combined response to the two order parameters. Additionally, we find that it is due to the anisotropy of the CDW gap, that the LES energy across  $T_c$ , reported by Ref. (14), varies as a function of  $\vec{k}$ , so that an isotropic multi-band superconductivity is a viable scenario for the low temperature ground state in NbSe<sub>2</sub>.

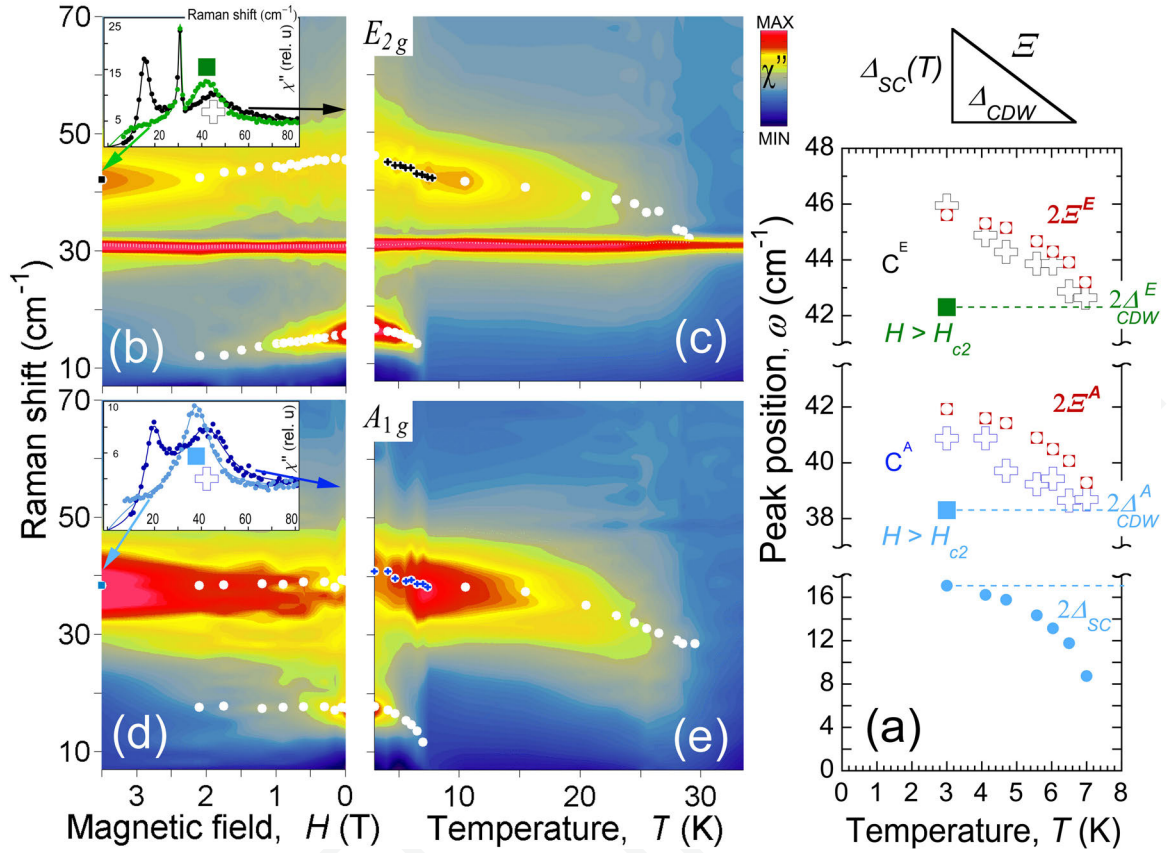


Figure 4: **Combined response from coexisting order parameters.** (a) Solid circles in the 10-20 cm $^{-1}$  range show the Raman shift position of the superconductivity induced  $G^A$  peak as a function of temperature (bottom). Crosses show the positions of the  $C^E$  (top) and the  $C^A$  (center) peaks as a function of temperature. Squares show the position of the same C peaks at 3 K in the presence of a 5 T magnetic field. Shaded circles show combination of the  $G^A$  peak and the  $C^{A,E}(H > H_{c2})$  peaks positions according to Eq. 1. The right angled triangle atop of (a) illustrates the relationship between the quantities  $\Delta_{SC}$ ,  $\Delta_{CDW}$ , and  $\Xi$ . Panels (b)-(e) show color coded polarization resolved Raman intensity generated with  $\lambda_L = 647$  nm as a function of magnetic field and as a function of temperature according to the axes labels. Insets in (b) and (d) show spectra for zero and 3.5 T magnetic field in the respective symmetry channels,  $E^{2g}$  and  $A^{1g}$ . The C peaks positions are marked with the same symbols as in (a) to distinguish the CDW+SC (cross) and CDW only (solid square) situations.

## Methods

**Experimental: Raman scattering.** In our experimental setup the incoming laser light was back scattered from either the *ab*-plane or the edge (*ca*-plane) of the NbSe<sub>2</sub> single crystals grown by iodine-vapor transport (31). The incident laser power of ca. 1 mW was focused to a 100 × 200 μm spot. The elastically scattered light was filtered by two subsequent monochromator stages combined in subtractive mode. The Raman part of the spectra was recorded with a CCD camera (Princeton Instruments) after passing a third monochromator stage (Acton). Circularly polarized light with parallel and opposite chiralities was used to select the A<sub>1g</sub> and E<sub>2g</sub> symmetry channels of the D<sub>6h</sub><sup>4</sup> space group in which the 2H polytype of NbSe<sub>2</sub> crystallizes. Linearly polarized light in the hh (parallel) and vh (cross) polarizer/analyzer settings was used to record ‘polarized’ (A<sub>1g</sub> + E<sub>2g</sub>) spectra from the *ab*-plane or ‘depolarized’ spectra from the edge (E<sub>1g</sub>). Cooling down to 1.7 K was provided by cold flowing helium gas inside a cryostat (Oxford Instruments). With temperature correction for the heating due to laser power dissipation this corresponds to the lowest accessible sample temperature of 3 K. The correction for the laser heating was based on available thermal conductivity data (32) and is described elsewhere (33).

**Theoretical: Electronic Structure Calculations.** The density functional calculations have been performed using a full-potential augmented plane wave + local orbitals approach (34). A Generalized Gradient Approximation scheme (35) was chosen to specify the exchange correlation potential. The hexagonal lattice constants were given as  $a = 3.44 \text{ \AA}$  and  $c = 12.55 \text{ \AA}$ , as measured (20). The muffin-tin radii were set to 1.22 Å and 1.16 Å for Nb and Se, respectively, with  $RK_{max} = 7.0$ . The spin-orbit coupling has been taken into account using a second variational method. We selected a fine mesh of  $73 \times 73 \times 15$  *k*-points to ensure a high resolution of the Fermi surface sheets and the Raman vertices thereon.

## Acknowledgements

We would like to acknowledge C. Kloc for providing the NbSe<sub>2</sub> crystal, and B. Nowadnick for valuable discussions. We thank T. Hanaguri for sharing his STM measurements prior to publication.

A.M. has been supported in parts by the German Natational Academic foundation, the Lucent foundation, Rutgers University, German Academic Foreign Exchange fund, and J. Plano foundation. I. S. has been supported by the Beckman foundation. A.T. acknowledges funding from the European Research Council under Grant No. FP7-ERC-227378 and from the EU-Indian network MONAMI grant.

## Authors contributions

A.M. has performed the Raman measurements, analyzed the data, and composed the manuscript. I.M. and A.T. have calculated the polarization dependent Raman vertices shown in Fig. 3. A. T. has calculated the band structure shown in Fig. 1 and co-written the manuscript. I. S. has assisted with the data analysis, drawn the figures, and co-written the manuscript. A. N. has formulated the Nambu-space representation of the CDW+SC order parameter and co-written the manuscript. B.D. has maintained the experimental setup and assisted with measurements. C. Kloc's student has grown the NbSe<sub>2</sub> crystal. G. B. has designed the experimental setup and supervised the project.

## References

- [1] Revolinski, E., Brown, B. E., Beerntsen, D. J., and Armitage, C. H. The selenide and telluride systems of niobium and tantalum. *Journal of less common metals* **8**, 63–72 (1965).
- [2] Marchevsky, M., Higgins, M. J., and Bhattacharya, S. Two coexisting vortex phases in the peak effect regime in a superconductor. *Nature* **409**(6820), 591 (2001).
- [3] Moncton, D. E., Axe, J. D., and DiSalvo, F. J. Study of superlattice formation in 2H-NbSe<sub>2</sub> and 2H-TaSe<sub>2</sub> by neutron scattering. *Physical Review Letters* **34**(12), 734 (1975).
- [4] Ando, H., Yokoya, T., Ishizaka, K., Tsuda, S., Kiss, T., Shin, S., Eguchi, T., Nohara, M., and Takagi, H. Angle-resolved photoemission study of K<sub>0.3</sub>MoO<sub>3</sub>: Direct observation of temperature-dependent Fermi surface across the Peierls transition. *Journal of Physics Condensed Matter* **17**, 4935 (2005).
- [5] Solovyeva, V., Cmyrev, A., Sachser, R., Reith, H., and Huth, M. Influence of irradiation-induced disorder on the Peierls transition in TTF-TCNQ microdomains. *Journal of Physics D: Applied Physics* **44**(38), 385301 (2011).
- [6] Antonets, S. I. and Timochko, B. M. Charge density waves in crystals. *Ukrainian Journal of Physics* **24**(5), 628–636, Mai (1979).
- [7] Berthier, C., Molinié, P., and Jérôme, D. Evidence for a connection between charge density waves and the pressure enhancement of superconductivity in 2H-NbSe<sub>2</sub>. *Solid State Communications* **18**(9/10), 1393 (1976).
- [8] Seibold, G. and Varlamov, S. Relationship between incommensurability and superconductivity in peierls distorted charge-density-wave systems. *Phys. Rev. B* **60**, 13056 (1999).
- [9] Klein, M. V. and Dierker, S. B. Theory of Raman scattering in superconductors. *Physical Review B* **29**(9), 4976 (1984).
- [10] Vanyolos, A. and Virosztek, A. Electronic Raman scattering in unconventional density waves. *Physical Review B* **72**(11), 115119 (2005).
- [11] Bilbro, G. and McMillan, W. L. Theoretical model of superconductivity and the martensitic transformation in A15 compounds. *Phys. Rev. B* **14**, 1887–1892, Sep (1976).
- [12] Littlewood, P. B. and Varma, C. M. Gauge-invariant theory of the dynamical interaction of charge density waves and superconductivity. *Physical Review Letters* **47**, 811 (1981).

- [13] Borisenko, S. V., Kordyuk, A. A., Zabolotnyy, V. B., Inosov, D. S., Evtushinsky, D., Buchner, B., Yaresko, A. N., Varykhalov, R. F. A., Eberhardt, W., Patthey, L., and Berger, H. Two energy gaps and Fermi-surface “arcs” in NbSe<sub>2</sub>. *Physical Review Letters* **102**, 166402 (2009).
- [14] Kiss, T., Yokoya, T., Chainani, A., Shin, S., Hanaguri, T., Nohara, M., and Takagi, H. Charge-order-maximized momentum-dependent superconductivity. *Nature Physics* **3**, 720 (2007).
- [15] Weber, F., Rosenkranz, S., Castellán, J.-P., Osborn, R., Hott, R., Heid, R., Bohnen, K.-P., Egami, T., Said, A. H., and Reznik, D. Extended phonon collapse and the origin of the charge-density wave in 2H-NbSe<sub>2</sub>. *Phys. Rev. Lett.* **107**, 107403, Sep (2011).
- [16] Murphy, B. M., Requardt, H., Stettner, J., Serrano, J., Krisch, M., Müller, M., and Press, W. Phonon modes at the 2H-NbSe<sub>2</sub> surface observed by grazing incidence inelastic X-ray scattering. *Physical Review Letters* **95**(25), 256104 (2005).
- [17] Tsang, J. C., Smith Jr., J. E., and Shafer, M. W. Raman spectroscopy of soft modes at the charge-density-wave phase transition in 2H-NbSe<sub>2</sub>. *Physical Review Letters* **37**(21), 1407 (1976).
- [18] Sooryakumar, R. and Klein, M. V. Raman scattering by superconducting-gap excitations and their coupling to charge-density waves. *Physical Review Letters* **45**, 660 (1980).
- [19] Rice, M. J. and Strässler, S. Theory of a quasi-one-dimensional band-conductor. *Solid State Communications* **13**(1), 125–128 (1973).
- [20] Marezio, M., Dernier, P. D., Menth, A., and Hull Jr., J. W. The crystal structure of NbSe<sub>2</sub> at 15° K. *Journal of Solid State Chemistry* **4**, 425–429 (1972).
- [21] Moncton, D. E., Axe, J. D., and DiSalvo, F. J. Neutron scattering study of the charge-density wave transitions in 2H – TaSe<sub>2</sub> and 2H – NbSe<sub>2</sub>. *Phys. Rev. B* **16**, 801, Jul (1977).
- [22] Rahnejat, K., Howard, C., Shuttleworth, N., Schofield, S., Iwaya, K., Hirjibehedin, C., Renner, C., Aeppli, G., and Ellerby, M. Charge density waves in the graphene sheets of the superconductor CaC<sub>6</sub>. *Nature Communications* **2**(558), 1–6 (2011).
- [23] Clayman, B. P. and Frindt, R. F. The superconducting energy gap of NbSe<sub>2</sub>. *Solid State Communications* **9**, 1881 (1971).

- [24] Hess, H. F., Robinson, R. B., Dynes, R. C., Valles Jr., J. M., and Waszczak, J. V. Scanning-tunneling-microscope observations of the Abrikosov flux lattice and the density of states near and inside a fluxoid. *Physical Review Letters* **62**, 214 (1989).
- [25] Sauer, C. and Blumberg, G. Screening of the Raman response in multiband superconductors: Application to iron pnictides. *Physical Review B* **82**(1), 014525 (2010).
- [26] Ismer, J.-P., Eremin, I., Rossi, E., Morr, D. K., and Blumberg, G. Theory of multiband superconductivity in spin-density-wave metals. *Phys. Rev. Lett.* **105**, 037003, Jul (2010).
- [27] Klein, M. V. Theory of Raman scattering from Leggett's collective mode in a multiband superconductor: Application to MgB<sub>2</sub>. *Physical Review B* **82**(1), 014507 (2010).
- [28] Stanev, V. Model of collective modes in three-band superconductors with repulsive interband interactions. *Phys. Rev. B* **85**, 174520, May (2012).
- [29] Blumberg, G., Mialitsin, A., Dennis, B. S., Klein, M. V., Zhigadlo, N. D., and Karpinski, J. Observation of Leggett's collective mode in a multiband MgB<sub>2</sub> superconductor. *Physical Review Letters* **99**(22), 227002 (2007).
- [30] T. Hanaguri, private communication.
- [31] Oglesby, C. S., Bucher, E., Kloc, C., and Hohl, H. Growth of faceted niobium diselenide. *Journal of Crystal Growth* **137**(1-2), 289 – 294 (1994).
- [32] Bel, R., Behnia, K., and Berger, H. Ambipolar Nernst effect in NbSe<sub>2</sub>. *Physical Review Letters* **91**, 066602 (2003).
- [33] Mialitsin, A. *Raman scattering from layered superconductors: effects of Charge-ordering, two-band superconductivity, and structural disorder*. PhD thesis, Rutgers, The State University of New Jersey, (2010).
- [34] Blaha, P., Schwarz, K., Madsen, G. K. H., Kvasnicka, D., and Luitz, J. *WIEN2k, An Augmented Plane Wave + Local Orbitals Program for Calculating Crystal Properties*. Karlheinz Schwarz, Techn. Universität Wien, Austria, (2001).
- [35] Perdew, J. P., Burke, S., and Ernzerhof, M. Generalized gradient approximation made simple. *Phys. Rev. Lett.* **77**(18), 3865, October (1996).